2014

Potential Of Controlling Subcooling In Residential A/C System

Lihan Xu
Air Conditioning and Refrigeration Center, University of Illinois at Urbana-Champaign, United States of America, lihanxu2@illinois.edu

Predrag S. Hrnjak
Creative Thermal Solution, pega@illinois.edu

Potential for Improving Efficiency by Controlling Subcooling in Residential A/C System

Lihan XU[1]*, Pega HRNJAK[1,2]

[1]Department of Mechanical Science and Engineering,
University of Illinois at Urbana-Champaign
Urbana, IL, USA
lihanxu2@illinois.edu
[2]Creative Thermal Solution
Urbana, IL, USA
pega@illinois.edu
* Corresponding Author

ABSTRACT

This paper presents effects of subcooling in condenser on efficiency of residential A/C systems in steady-state. To explore these effects, a system model with detailed component models was developed. The model was validated using experiments conducted on a typical 3 Ton (10.5 kW) system that used R410A. After validation, the model was used to evaluate the effects of subcooling in a range of operating conditions and several condenser sizes. The model results indicate that subcooling control can improve the system efficiency up to 8% for a given operating condition. Also, the improvements in efficiency are affected by condenser size. Smaller size of condenser results in greater potential for improvements. In addition, this paper presents a control strategy for achieving COP or cooling capacity Q maximizing subcooling as conditions vary.

1. INTRODUCTION

The potential for improving the system performance by controlling subcooling has already been investigated by Pottker and Hrnjak (2012) who showed that condenser subcooling can improve the mobile air-conditioning (MAC) system efficiency by 9% and 19% using R134a and R1234yf, respectively. In that study, evaporator and condenser air inlet temperature were 30℃ and 35℃ and were kept constant. The degree of subcooling was varied from 0 ℃ to 18℃ by adding refrigerant charge to the system. The results showed that there was a COP maximizing condenser subcooling for both refrigerants, at 9℃ for R134a and 11℃ for R1234yf. The objective of this paper is to transfer that finding to residential air-conditioning (RAC) system. If that potential is identified and quantified, then how do we control subcooling? Also, how does the system with subcooling control react to different operating conditions? What is the relationship between size of condenser and subcooling controlled COP improvement? These questions will be studied in this paper numerically first and then validated using experimental data from Beaver et al. (1999).

The mechanism of the way subcooling affects the vapor-compression refrigeration cycle is explained by comparing cycles with and without subcooling on a T-h diagram (Fig. 1). The blue solid line represents the refrigeration cycle without subcooling while the red dash line represents cycle with subcooling. For cycle without subcooling, the specific enthalpy change of evaporation is denoted by q (from 5 to 2) and specific compression work is denoted by w (from 2 to 3). 1 to 2 represents the evaporator superheat region. When subcooling is present in condenser, it results in both higher condensing temperature and lower refrigerant temperature at condenser outlet. Higher condensing temperature is mainly due to the reduction of the two-phase condensation region, and it consequently increases the specific compression work by Δw. The lower condenser exit temperature results in an increment in specific enthalpy difference by Δq. The increments Δq and Δw will change as subcooling varies. Considering the system efficiency, COP of cycle without subcooling is q/w while it is $(q + \Delta q)/(w + \Delta w)$ for cycle with subcooling. Therefore, the two effects compete; subcooling effect on system performance is the trade-off between the higher cooling capacity and higher compression work.

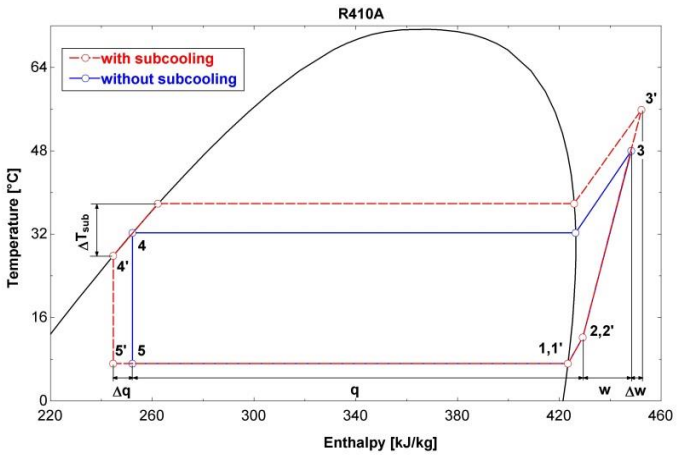

Figure 1: Temperature-specific enthalpy diagram of vapor-compression refrigeration cycle with/without subcooling

2. SYSTEM DESCRIPTION

The components of the 3 Ton (10.5 kW) system studied in this paper are a high efficiency round-tube R410A A/C & H/P outdoor coil, a round-tube evaporator with installed TXV (thermostatic expansion valve), and a hermetic scroll compressor. The specifications of the evaporator and condenser are listed in Table 1 (Beaver et al., 1999).

Table 1: A/C system component specifications

	Condenser	**Evaporator**
Description	One row, two circuits, fin pitch 1 mm (24 fpi)	Three rows, six circuits, fin pitch 1.7 mm (14 fpi)
Face area	1.42 m^2	0.32 m^2
Core depth	0.0185 m	0.056 m
Core volume	0.026 m^3	0.018 m^3
Airside area	44.56 m^2	18.88 m^2
Ref. side area	1.58 m^2	1.08 m^2
Material	Aluminum wavy plate fins, copper tubes, OD=9.5 mm	Aluminum wavy plate fins, copper tubes, OD=9.5 mm

3. SIMULATION MODEL DESCRIPTION AND VALIDATION

In order to predict the performance of the residential A/C system, a comprehensive model has been built using EES (Engineering Equation Solver). The system model contains modules simulating the four main components: condenser, expansion valve, evaporator, and compressor. They are coupled by correlating equations of pressure, enthalpy, and mass flow rate. For the heat exchangers, the finite volume method was used for calculating the heat transfer rate and pressure drop. Each tube pass of condenser was divided into 5 elements while 3 elements per tube pass were used for the evaporator. For each element, the effectiveness-NTU method for a cross-flow heat exchanger was applied for heat transfer calculations. Detailed heat transfer and pressure drop correlations are listed in Table 2.

For the compressor model, the 10-parameter polynomial curve fitting method was adopted. Using the manufacturing data, mass flow rate and compressor power can be calculated. A scaling factor β was used to adjust the speed of the variable-speed compressor in the model.

The inputs to the system model are: heat exchanger and compressor geometries, air volumetric flow rate through outdoor and indoor chamber ducts, air-side inlet conditions, and degrees of superheat and subcooling. The modules run separately in a sequential order, which output thermodynamic properties such as temperature, pressure, and

specific enthalpy when the system inputs were implemented.

Several other assumptions were made for the model:

1. Uniform temperature and velocity profile at air-side inlet.
2. Isenthalpic expansion process.
3. Volumetric and isentropic efficiencies are independent of compressor speed.
4. Refrigerant pressure drop in compressor discharge line and liquid line are ignored.

Table 2: Heat transfer and pressure drop correlations

Items	Correlations
Refrigerant-side	
Single phase HTC	Gnielinski (1976)
Condensation HTC	Cavallini et al. (2006)
Evaporation HTC	Wattelet and Chato (1994)
Single-phase pressure drop	Friction factor from Churchill (1977)
Two-phase pressure drop	Friedel (1979)
Air-side	
HTC for wavy plate fin-and-tube HX	Webb (1990)
Pressure drop for wavy plate fin-and-tube HX	Kim, Yun and Webb (1997)

The model was then validated using experimental data from a previous study (Beaver et al., 1999). Three operating conditions were tested (listed in Table 3). Indoor temperature was kept the same for all three conditions while outdoor temperature varied. Condition A and B are prescribed by ASHARE Standard 116/1995 (1995).

Table 3: Test conditions

	T_{eai} [℃]	T_{cai} [℃]	RH	AFR (indoor) $[m^3/s]$	AFR (outdoor) $[m^3/s]$	ΔT_{sub} [℃]	ΔT_{sup} [℃]
A	26.7	35.0	0.506	0.57	1.33	6.9	2.9
B	26.7	27.8	0.320	0.57	1.33	6.7	3.0
C	26.7	39.0	0.504	0.57	1.33	6.3	0.6

The results from simulation and experimental data from Beaver et al. (1999) were compared in Table 4 for the operating conditions listed in Table 3. Most of the simulation results were within 2% of error while the error of saturation temperatures are within ± 1.6 ℃ .

Figure 2 shows model validation by comparing experimental data (blue solid line) and simulation results (red dash line) in a P-h diagram for condition **B**.

Table 4: Model validation

	Condition A			Condition B			Condition C		
	Model	Data	Error	Model	Data	Error	Model	Data	Error
Q_e [W]	10.40	10.46	-0.57%	10.49	10.50	-0.10%	10.06	10.00	0.60%
Q_c [W]	12.93	13.10	-1.30%	12.58	12.61	-0.24%	12.85	13.01	-1.23%
W_{cpr} [W]	2.63	2.64	-0.38%	2.22	2.20	0.91%	2.86	2.88	-0.69%
T_{evap} [℃]	8.9	10.5	-1.6 ℃	6.4	7.5	-1.1 ℃	9.8	11.3	-1.5 ℃
T_{cond} [℃]	46.0	44.9	1.1 ℃	38.4	37.0	1.4 ℃	49.6	48.6	1.0 ℃
COP	3.96	3.97	-0.25%	4.72	4.76	-0.84%	3.52	3.47	1.44%

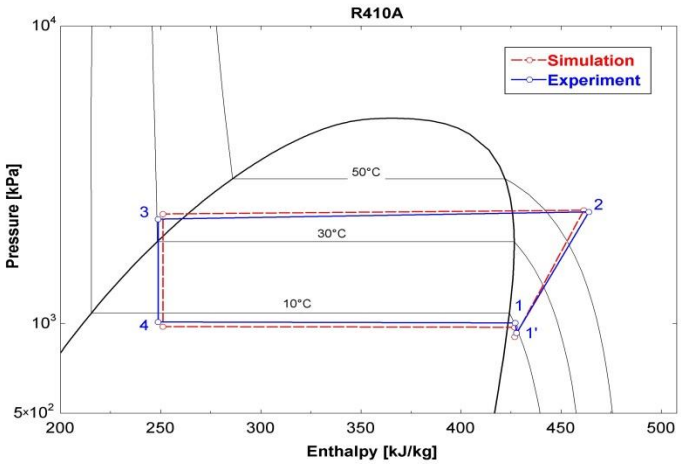

Figure 2: Pressure-specific enthalpy diagram (condition **B** in Table 3)

4. SIMULATION RESULTS

The model validated above will help to analyze subcooling effects in more realistic situations than a pure thermodynamic cycle. Figure 3 (a) shows the effects of subcooling on normalized COP, cooling capacity, and compression work for condition **A** (Table 3) of the system described in section 3. The normalization was done based on values at zero subcooling. For this operating condition, subcooling temperature was varied from 0 to 12 ℃ while air flow rate, evaporator outlet superheat, and compressor speed were kept constant. As subcooling increases from 0 to 12 ℃, both cooling capacity and compression work increase while COP experiences its maximum value at ΔT_{sub} = 6.5 ℃. The interaction between capacity and work determines the shape of the COP curve. This result confirms the cycle analysis in previous section, where it was explained that increase in subcooling results in both higher condensing temperature and lower refrigerant temperature at condenser outlet, resulting in higher specific enthalpy difference in evaporator and higher specific compressor work. As subcooling increases, refrigerant mass flow rate also decreases as a consequence of lowering evaporation pressure (see Fig. 4) and this was accounted for the cooling capacity and work calculations. The increase of cooling capacity slows down while the increase of compression work accelerates when passing the COP maximizing subcooling temperature. This indicates that subcooling has a stronger effect on cooling capacity from zero to COP maximizing subcooling and inversely for subcooling above COP maximizing value.

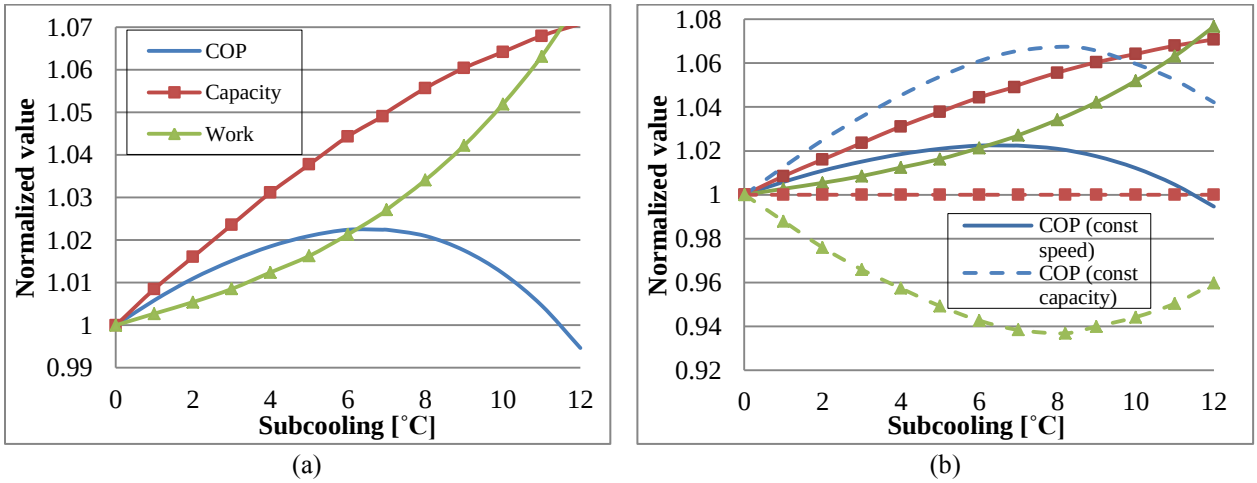

Figure 3: (a) Effect of subcooling temperature on normalized COP, cooling capacity, and compression work for constant compressor speed; (b) Comparison of subcooling effects on normalized COP, cooling capacity and compression work for constant compressor speed and constant cooling capacity (condition **A** in Table 3)

A similar analysis was conducted for keeping cooling capacity constant instead of compressor speed. Capacity was matched at zero subcooling. Figure 3 (b) shows the comparison of subcooling effects on normalized COP, cooling capacity, and compression work of constant speed case and constant cooling capacity case. The improvement of system COP is much higher for the constant cooling capacity case than that of constant compressor speed. This is because for the constant cooling capacity case, the increase in cooling capacity when compressor speed is constant as shown in Figure 3 (a) is now accounted in COP improvement.

Figure 5 presents the effect of subcooling on normalized COP for three condenser air inlet temperatures 27.8 ℃, 35℃, and 39 ℃ while evaporator air inlet temperature was kept to be 26.7 ℃ (condition **A, B, C** in Table 3). Subcooling temperature was varied from 0 to 12℃ while air flow rates and superheat were kept constant (specified in Table 3). Cooling capacity was matched at zero subcooling case for each operating condition by adjusting the compressor speed. The three operating conditions all show the same subcooling effects on COP, but the improvements are different. The COP improvement is 7.9% (at ΔT_{sub}=9.0℃), 6.7% (at ΔT_{sub}=8.2 ℃) and 5.3% (at ΔT_{sub}=8.0℃) for T_{cai} equal to 39 ℃ , 35℃, 27.8 ℃ , respectively. Higher condenser air inlet temperature results in greater COP improvements by changing subcooling.

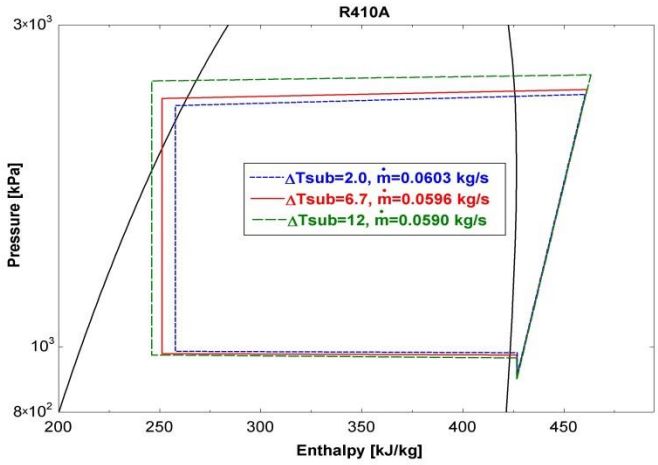

Figure 4: Effect of subcooling on refrigerant mass flow rates for ΔT_{sub}=2.0 ℃, 6.7 ℃, and 12 ℃

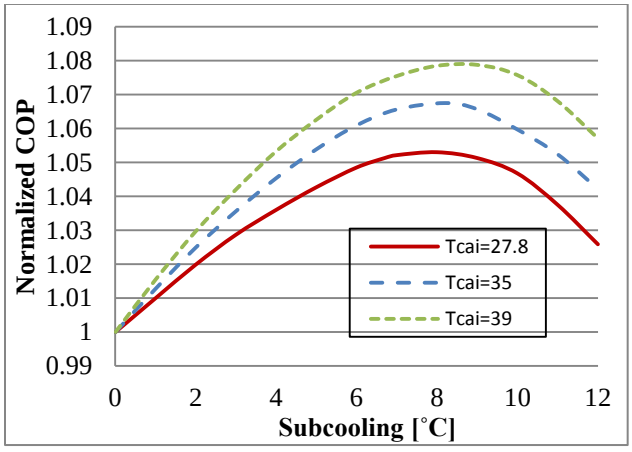

Figure 5: Effect of subcooling temperature on normalized COP (condition **A, B, C** in Table 3) for constant capacity

The simulation results indicate that the subcooling effect on RAC system performance is not as high as in MAC as predicted by Pottker and Hrnjak (2012). The main reason for that is due to the much larger condenser size in RAC compared to MAC. In fact, condenser size has a strong impact on the subcooling effect. The simulation model was used to evaluate the magnitude of the condenser size effects in the next section.

5. CONDENSER SIZE EFFECT

Condenser size effects on subcooling improved system efficiency were studied by varying the condenser size to be 1, 2, and 4 times the original condenser size (A) specified in system description of section 2 (air-side area A_a=44.56 m^2, refrigerant-side area A_r=1.58 m^2) by adjusting the condenser side geometry. Condenser air-side face velocity was kept constant by increasing the outdoor air volumetric flow rate by the same factor as geometry to maintain constant air-side heat transfer. The volumetric flow rate is 1.33 m^3/s. Multiplying volumetric flow rates 2 and 4 times may not be realistic in reality, but we selected that option for the purpose of analyzing size effects. Everything else such as evaporator size and indoor air volumetric flow rate were kept constant. Operating condition **A, B, C** (Table 3) were applied for this analysis. Simulation results for condition **B** (Fig. 6 and Table 5) show that larger the condenser size, smaller subcooling effect on system performance is observed. For the original condenser size, subcooling can improve the system efficiency by 5.3%, whereas for 4 times original condenser size, subcooling effect becomes detrimental to COP. Also, for different condenser sizes, COP maximizing subcooling temperature varies. It decreases from 8.0 ℃ (original size A) to 4.0 ℃ (2 times A), then further to 0.2 ℃ (4 times A). The similar findings also apply for operating conditions **A** and **C**.

Effect of condenser size on subcooling improved cooling capacity Q was also studied. Simulation results for condition **B** (Table 3) are shown in Figure 7 and Table 6 (similar findings for conditions **A, C**). **S**imilar to COP, smaller condenser size has higher potential for increasing cooling capacity. For the original condenser size, the improvement was 5.6%, while it decreased to 2.2% as condenser size doubled, and no improvement when condenser size quadrupled. Q maximizing subcooling temperature also decreases as condenser size increases.

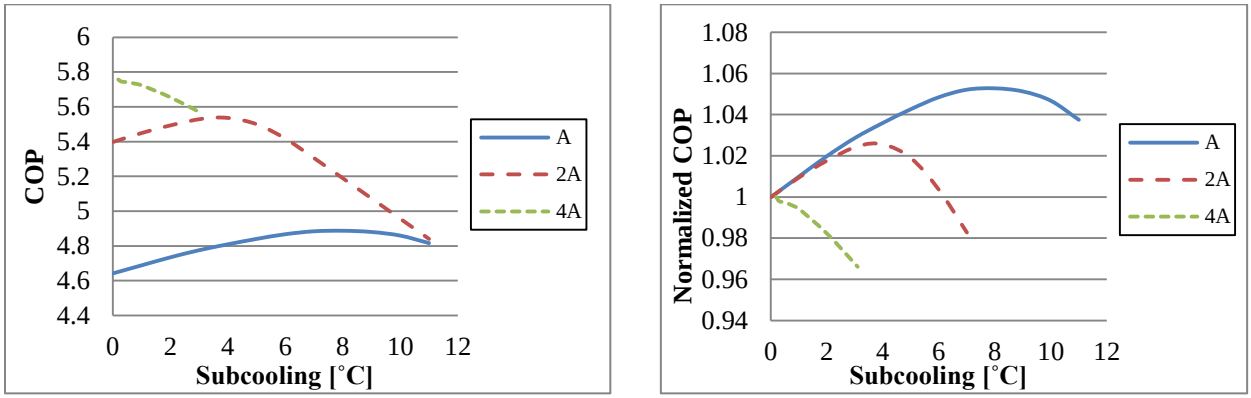

(a) (b)

Figure 6: Effect of condenser size on subcooling improved COP presented in (a) actual and (b) normalized terms (condition **B** in Table 3)

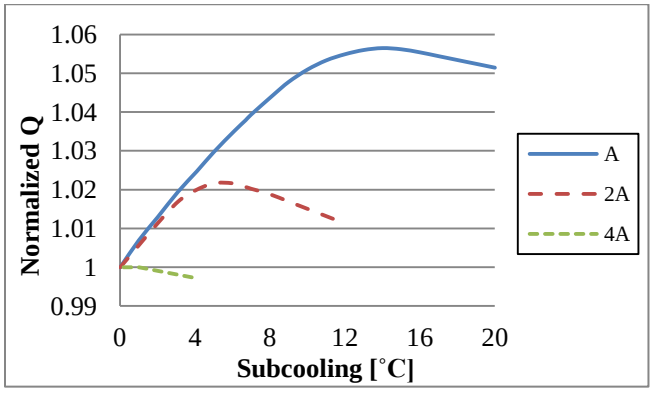

Figure 7: Effect of condenser size on subcooling improved cooling capacity Q presented in normalized way (condition **B** in Table 3)

Subcooling effect is very sensitive to condenser size because it is inversely proportional to condenser air inlet temperature difference ΔT_{in} (i.e. difference between condensing temperature and condenser air inlet temperature). In fact, condenser size effects can be interpreted as effects of ΔT_{in} on subcooling improved efficiency or cooling capacity. Smaller condenser size results in higher ΔT_{in} and thus greater room for condenser subcooling and consequently greater potential for COP or Q improvements.

Tables 5 and 6 summarize COP and Q maximizing subcooling temperature ΔT_{sub} and its corresponding condenser air inlet temperature difference ΔT_{in} from simulation results, respectively. Both COP and Q maximizing subcooling temperature exhibit an inverse relationship with condenser size, i.e. direct relationship with ΔT_{in}. In fact, ΔT_{sub} depends linearly on ΔT_{in}. COP or Q maximizing subcooling can be presented as a linear function of ΔT_{in}: $\Delta \boldsymbol{T_{sub}} = \boldsymbol{A^*} \Delta \boldsymbol{T_{in}} + \boldsymbol{B}$. The coefficients A and B can be determined based on available data for a certain range of conditions.

Table 5: COP maximizing subcooling temperature and condenser air inlet temperature difference for varying condenser sizes (condition **A, B, C** in Table 3)

Condenser size	Condition A		Condition B		Condition C	
	ΔT_{sub} [°C]	ΔT_{in} [°C]	ΔT_{sub} [°C]	ΔT_{in} [°C]	ΔT_{sub} [°C]	ΔT_{in} [°C]
A	8.2	11.2	8.0	10.7	9.0	11.6
2A	4.0	4.7	4.0	4.4	4.0	4.7
4A	0.3	0.2	0.2	0.3	0.4	0.5

Table 6: Q maximizing subcooling temperature and condenser air inlet temperature difference for varying condenser sizes (condition **A, B, C** in Table 3)

Condenser size	Condition A		Condition B		Condition C	
	ΔT_{sub} [°C]	ΔT_{in} [°C]	ΔT_{sub} [°C]	ΔT_{in} [°C]	ΔT_{sub} [°C]	ΔT_{in} [°C]
A	16.0	16.6	14.0	14.6	18.0	18.2
2A	6.9	7.0	5.5	5.6	6.3	6.4
4A	0.9	1.0	0.2	0.3	0.6	0.8

6. SUBCOOLING CONTROL STRATEGY

It would be reasonable to evaluate possibility in improving performance of the system (COP or capacity) by controlling subcooling. That could be achieved by controlling opening of the expansion valve based on subcooling and utilizing low-pressure receiver option. Low-pressure receiver (accumulator) would be beneficial for reversible system. We will discuss below a strategy for controlling such a valve.

6.1 Maximization of COP

Results indicate that COP maximizing subcooling can be presented as a linear function of condenser inlet temperature difference ΔT_{in}: $\Delta \boldsymbol{T_{sub}} = \boldsymbol{A^*} \Delta \boldsymbol{T_{in}} + \boldsymbol{B}$. Using simulation results for three operating conditions **A, B, C** in Table 3 (T_{eai}=26.7°C, T_{cai}=27.8 °C, 35°C and 39 °C) and three condenser sizes (1, 2 and 4 times of original area A), a quantified relationship was proposed by curve fitting: $\Delta \boldsymbol{T_{sub}} = \boldsymbol{0.739^*} \Delta \boldsymbol{T_{in}} + \boldsymbol{0.227}$ (shown in Fig. 8). With this relationship, COP maximizing subcooling temperature can be obtained for the specified conditions.

6.2 Maximization of cooling capacity Q

Same logic could be applied on the same simulation results as in section 6.1. Quantified relationship between Q maximizing subcooling temperature ΔT_{sub} and condenser air inlet temperature difference ΔT_{in} is presented by linear equation: $\Delta \boldsymbol{T_{sub}} = \boldsymbol{1.0237^*} \Delta \boldsymbol{T_{in}} + \boldsymbol{0.0373}$ (shown in Fig. 9). With this relationship, cooling capacity maximizing subcooling can be obtained for varying conditions.

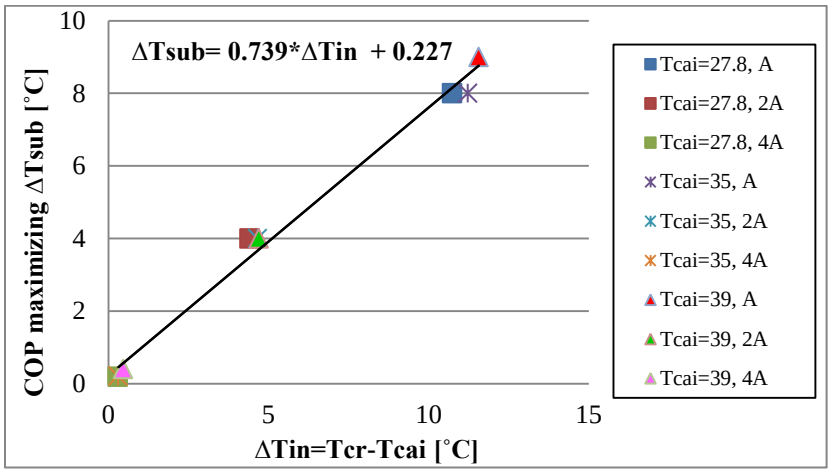

Figure 8: COP maximizing ΔT_{sub} as a function of ΔT_{in}

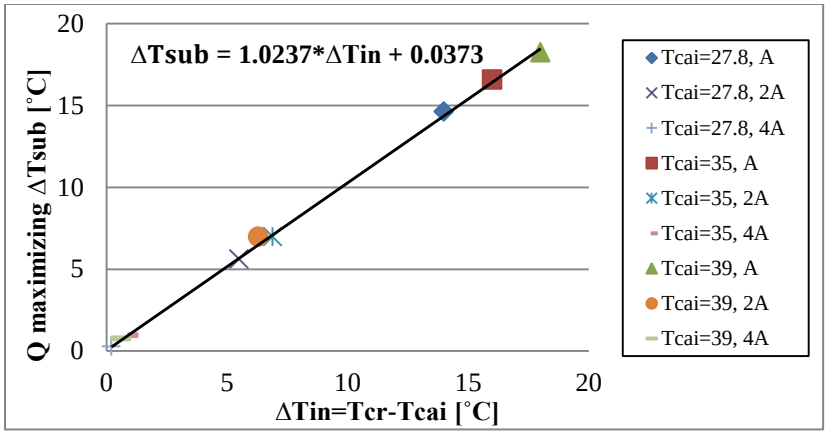

Figure 9: Q maximizing ΔT_{sub} as a function of ΔT_{in}

6.3 Possible Control Strategy

In principle there could be two objective functions for controlling subcooling: maximization of capacity Q and maximization of COP. In text above we have presented COP maximizing and Q maximizing values of subcooling. The correlations hold for a range of component sizes (1, 2 and 4 times of original condenser size A specified in section 5) and operating conditions (**A, B, C** in Table 3). If indicated values are attractive, a control can be obtained using an EXV (electronic expansion valve) after condenser to provide optimal subcooling for each condition. The strategy for controlling valve position can be based on maximization of capacity when needed (at the cool-downs or very high loads) followed by efficiency maximization once it is determined that capacity is sufficient.

The efficiency optimization procedure is presented in the flow chart in Figure 10. Based on measurements of condenser air inlet temperature T_{cai}, condensing temperature T_{cr}, and condenser refrigerant outlet temperatureT_{cro}, condenser air inlet temperature difference ΔT_{in} will be calculated. The COP maximizing subcooling value will be determined from the equation $\Delta T_{sub} = 0.739 * \Delta T_{in} + 0.227$ (Fig. 8) and compared with the actual subcooling temperature. If the actual value is bigger than the curve-fitting value, subcooling needs to be decreased. EXV will be adjusted in the direction of opening it more so that condensing pressure will decrease. The lowering of condensing pressure will enlarge the two-phase region of condenser during heat transfer and thus reduce subcooling. Vice versa for the case that actual subcooling is smaller than the ideal value. EXV needs to be adjusted in the direction of closing it. If capacity is not sufficient, maximization of capacity will be applied. The capacity optimization procedure is the same as efficiency optimization except that the Q maximization subcooling value is calculated using equation $\Delta T_{sub} = 1.0237 * \Delta T_{in} + 0.0373$ (Fig. 9). If automatic adjusting of EXV can be achieved, the residential a/c system will be able to maintain COP or Q maximizing subcooling when conditions change.

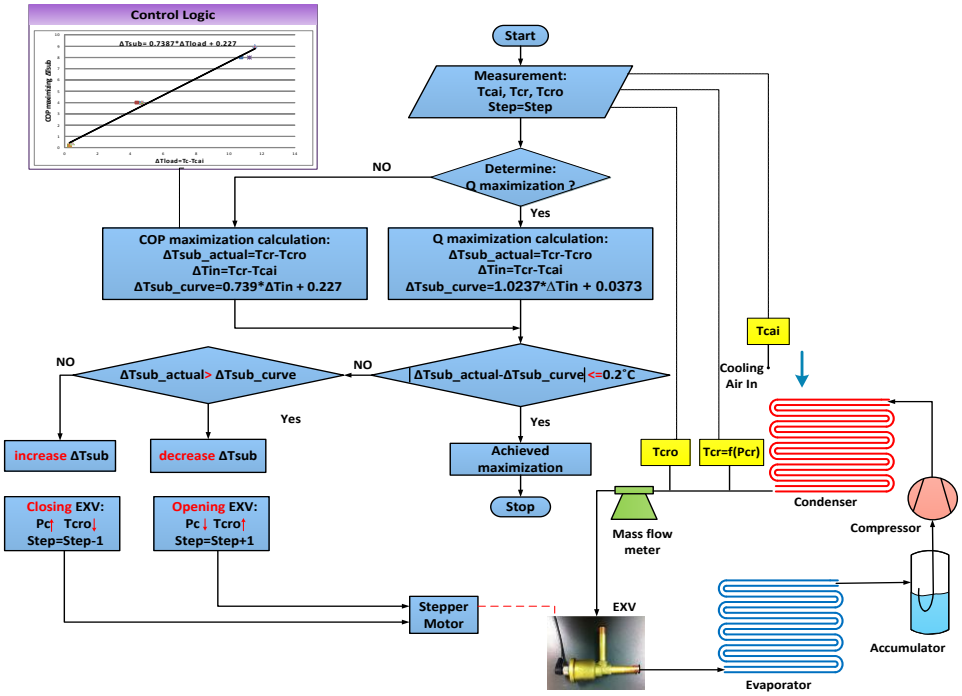

Figure 10: Control strategy

7. CONCLUSIONS AND FUTURE WORK

In conclusion, from the numerical study we have shown that controlling subcooling can improve the efficiency of a residential air-conditioning system up to 8%. The improvement is not as high as Pottker and Hrnjak (2012) achieved in an automotive air-conditioning system, due to the much larger condenser size of residential air-conditioning system. The simulation model was also used to evaluate the magnitude of the condenser size effect. The results indicated that smaller size of condenser is more sensitive to subcooling effects because smaller condenser size results in larger condenser air inlet temperature difference ΔT_{in} and consequently allows for greater room for improvement. For the residential air-conditioning system in this study, which has condenser air-side area of 44.56 m^2, controlling subcooling can improve the system COP by 5.3% and cooling capacity Q by 5.6% under operating condition **B**. When condenser size is doubled, the subcooling effects on system efficiency and cooling capacity become smaller. When it was quadrupled, the effects are insignificant. Also, COP or Q maximizing subcooling temperature can be represented as a linear function of condenser air inlet temperature difference ΔT_{in}, and subcooling can be controlled to achieve the optimal value. This paper proposed one way of controlling subcooling using an EXV. In reality, the charge of the system is usually set; the condition changes, subcooling may not be at the COP or Q maximizing value. Thus if automatic control of subcooling can be achieved, COP or Q maximization will be ensured. The effects of subcooling on system efficiency and cooling capacity improvements and the feasibility of the control scheme will be demonstrated using experiments, and further results will be revealed in the next paper.

REFERENCES

ANSI/ASHRAE Standard 116, 1995. Method of testing for seasonal efficiency of unitary air-conditioners and heat pumps, Proceeding American Society of Heating, Refrigeration and Air-Conditioning Engineers.

Beaver, A.C., Yin, J.M., Bullard, C.W., Hrnjak, P.S., 1999. An experimental investigation of transcritical carbon dioxide systems for residential air conditioning. *University of Illinois at Urbana-Champaign*, ACRC CR-18.

Cavallini, A., Del Col, D., Doretti, L., Matkovic, M., Rossetto, L., Zilio, C.,Censi, G., 2006. Condensation in horizontal smooth tubes: a new heat transfer model for heat exchanger design, *Heat Transfer Engineering* 27 (8), 31-38.

Churchill, S.W., 1977. Friction-factor equation spans all fluid-flow regimes, *Chemical Engineering* 84.

Friedel, L., 1979. Improved friction pressure drop correlations for horizontal and vertical two phase pipe flow. *In: European Two Phase Flow Group Meeting*, Italy, Paper E2.

Gnielinski, V., 1976. New equations for heat and mass transfer in turbulent pipe and channel flow, International *Chemical Engineering* 16, 359–368.

Kim, N.H., Yun, J.H., Webb, R.L., 1997, "Heat transfer and friction correlations for wavy plate fin-and-tube heat exchangers, *Transactions of ASME*, vol. 119, 560-567.

Pottker, G, Hrnjak, P.S., 2012. Effect of condenser subcooling of the performance of vapor compression systems: experimental and numerical investigation, *Proceedings of the Purdue Refrigeration and Air Conditioning Conference*, 169-176.

Wallelet, J.P. et al., 1994. Heat transfer flow regimes of refrigerants in a horizontal-tube evaporator, *University of Illinois at Urbana-Champaign*, ACRC TR-55.

Webb, R.L., 1990. Air-side heat transfer correlations for flat and wavy plate fin-and tube geometries, *ASHRAE Transactions*, Vol.96, 445-449.

NOMENCLATURE

COP	coefficient of performance	(-)	**Subscript**	
q	specific enthalpy difference across the evaporator	(kJ/kg)	e	evaporator
Q	capacity	(kW)	c	condenser
w	specific compression work	(kJ/kg)	cpr	compressor
W	work	(kW)	evap	evaporating
ṁ	mass flow rate	(kg/s)		
TXV	thermostatic expansion valve		cond	condensing
EXV	electronic expansion valve		a	air-side
fpi	fins per inch	(-)	r	refrigerant-side
HTC	heat transfer coefficient	(kW/m^2-k)	i	inlet
HX	heat exchanger		o	outlet
T	temperature	(℃)	sub	subcooling
ΔT	temperature difference	(℃)	in	condenser air inlet
RH	relative humidity	(-)		
AFR	air flow rate	(m^3/s)		
A	area	(m^2)		

.

ACKNOWLEDGEMENT

The authors thankfully acknowledge the support provided by the Air Conditioning and Refrigeration Center at the University of Illinois at Urbana-Champaign.